iScience

CellPress
OPEN ACCESS

Article

Mechanically-gated electrochemical ionic channels with chemically modified vertically aligned gold nanowires

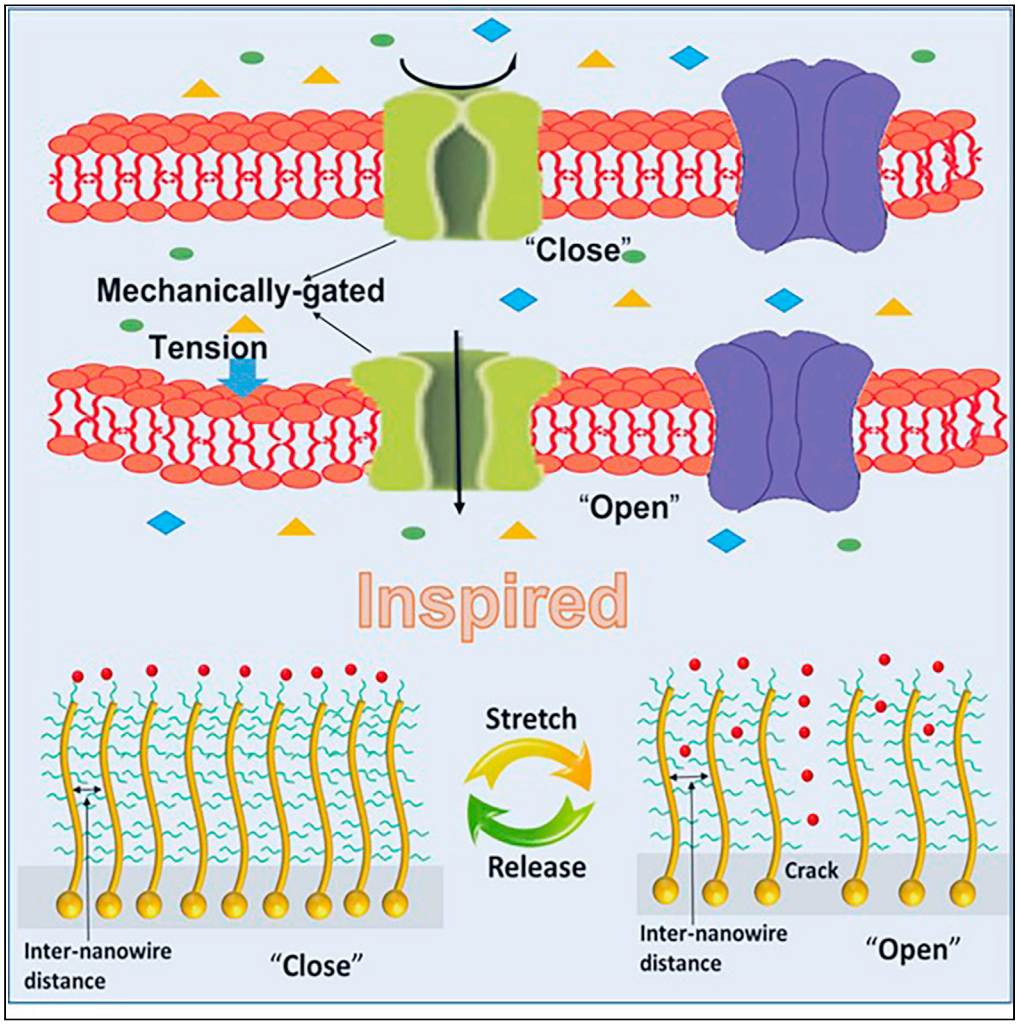

Qingfeng Zhai, Ren Wang, Quanxia Lyu, Yiyi Liu, Lim Wei Yap, Shu Gong, Wenlong Cheng

wenlong.cheng@monash.edu

Highlights

Bio-inspired strain-gated ionic channel is demonstrated on v-AuNWs electrode

v-AuNWs structures and DDT SAMs are crucial for the ionic gating behavior

Current response is a tradeoff between ionic channel and electrode conductivity

Bio-inspired mechanical switch is reversible and can be cycled for multiple cycles

Zhai et al., iScience *24*, 103307
November 19, 2021
https://doi.org/10.1016/j.isci.2021.103307

iScience

CellPress
OPEN ACCESS

Article

Mechanically-gated electrochemical ionic channels with chemically modified vertically aligned gold nanowires

Qingfeng Zhai,[1,2] Ren Wang,[1,2] Quanxia Lyu,[1,2] Yiyi Liu,[1,2] Lim Wei Yap,[1,2] Shu Gong,[1,2] and Wenlong Cheng[1,2,3,*]

SUMMARY

Mechanically-gated ion channels play an important role in the human body, whereas it is challenging to design artificial mechanically-controlled ionic transport devices as the intrinsically rigidity of traditional electrodes. Here, we report on a mechanically-gated electrochemical channel by virtue of vertically aligned gold nanowires (v-AuNWs) as 3D stretchable electrodes. By surface modification with a self-assembled 1-Dodecanethiol monolayer, the v-AuNWs become hydrophobic and inaccessible to hydrated redox species (e.g., $Fe(CN)_6^{3-/4-}$ and $Ru(bpy)_3^{2+}$). Under mechanical strains, the closely-packed v-AuNWs unzip/crack to generate ionic channels to enable redox reactions, giving rise to increases in Faradaic currents. The redox current increases with the strain level until it reaches a certain threshold value, and then decreases as the strain-induced conductivity decreases. The good reversible "on-off" behaviors for multiple cycles were also demonstrated. The results presented demonstrate a new strategy to control redox reactions simply by tensile strain, indicating the potential applications in future soft smart mechanotransduction devices.

INTRODUCTION

Human perceives the external world via our unique sensory system, in which specific cell-binding proteins can recognize and convert external stimuli (e.g., light, temperature, voltage, force, etc) into electrical signal (Baluška and Mancuso, 2009; Ranade et al., 2015). This is achieved via pore-forming membrane proteins, which allows specific ions to pass through the pores in response to specific stimuli. This leads to specific action potential responsible for the electrical signal generation and communication (Courtemanche et al., 1998; Reeh, 1986). Ionic channels are ubiquitous and present in membranes of all cells in biology, and various gated ion channels exist in our sensory system to respond to various external stimuli. Mechanically-gated ion channels are responsible for sensing touch, pressure and acoustic in biology (Delmas and Coste, 2013; Ranade et al., 2015).

To understand how membrane proteins gate ionic channels, supported lipid membranes have been constructed on electrochemical electrodes. Wang and co-workers developed a series of supported lipid membranes on solid electrodes and investigated the ion channel behaviors. For example, by modification of didodecyldimethylammonium bromide bilayer lipid membranes on glassy carbon electrode, the ion channel behavior of the supported bilayer lipid membrane with distinct channel current by using perchlorate anions as the stimulus and ruthenium(II) complex cations as the marker ions was demonstrated (Wu et al., 2000). In addition, by using ruthenium (II) as the maker ion, the ion channel behavior of amphotericin B in supported phosphatidylcholine bilayer model membranes was also investigated through electrochemistry and spectroscopy (Huang et al., 2002). In a recent study, Pappa et al. demonstrated a multimodal (optical and electronic) ion-channel activity in human-derived membranes, where TREK-1 ion-channel was expressed within supported lipid bilayers and PEDOT:PSS-based organic electrochemical transistors were used for combined optical and electronic measurements (Pappa et al., 2020). It has to be noted that all these electrochemical studies are based on bulk and rigid electrodes. Previous demonstrations are typically based on chemical and light stimuli; however, it has not yet been realized as a mechanical stimulus, to the best of knowledge, because of the rigidity nature of traditional electrochemical electrodes which are intrinsically not stretchable.

[1]Department of Chemical Engineering, Monash University, Clayton, VIC 3800, Australia

[2]New Horizon Research Centre, Monash University, Clayton, VIC 3800, Australia

[3]Lead contact

*Correspondence: wenlong.cheng@monash.edu

https://doi.org/10.1016/j.isci.2021.103307

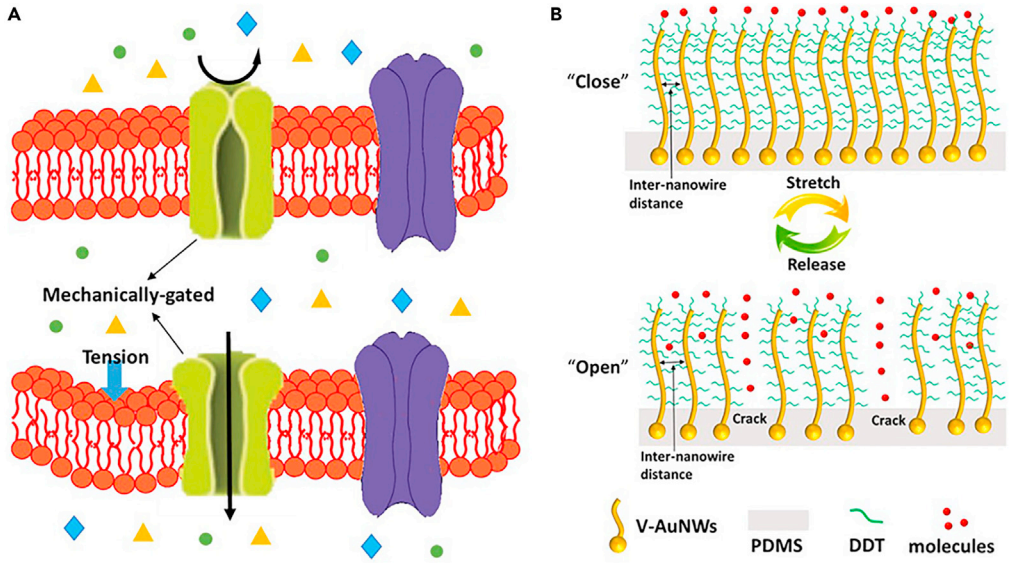

Figure 1. Schematic illustrations of inspired mechanically-gated ion channel

(A) Mechanically-gated ion channels in biological systems.

(B) Mechanical strain-gated electrochemical ionic channel based on v-AuNWs stretchable electrode.

Recently, we have developed a wet chemistry approach to fabricate stretchable electrode by using the vertically aligned gold nanowires (v-AuNWs), which could serve as an unconventional electrochemical platform for soft wearable sensors for detecting strains (Yap et al., 2019), pressures (Wang et al., 2021), temperature (Gong et al., 2019), and biological markers (Zhai and Cheng, 2019; Zhai et al., 2019, 2020a, 2020b). Here, we further demonstrate a mechanically-gated electrochemical ionic channel based on chemically modified v-AuNWs with 1-Dodecanethiol (DDT) (Figure 1). Note that self-assembled monolayer (SAM) of alkyl thiols on traditional gold electrodes has been widely investigated for bioelectrochemistry and biosensors (Dong and Li, 1997). However, the previous electrodes were not stretchable. We discovered that DDT-modified v-AuNWs electrodes exhibited mechanically-gated redox behaviors toward non-absorbing electrochemical probes including negatively charged $Fe(CN)_6^{3-/4-}$ and positively charged $Ru(bpy)_3^{2+}$ - a capability impossible to achieve with traditional rigid electrodes. The gating phenomenon shares analogy to cell membrane-binding proteins that can regulate ionic transports. Under non-strained states, the DDT SAMs passivity exposes surfaces of v-AuNWs electrode preventing from its electron communications with redox probes. This is termed as "close" state; whereas under the mechanical force such as strains, the v-AuNWs can unzip/crack to generate channels allowing hydrated redox probes to penetrate, which enables their electron transfer corresponding to an "open" state. The "open" state current is dependent on the external strain applied. In addition, the mechanically-gated electrochemical "close" and "open" states are reversible.

RESULTS AND DISCUSSION

DDT-modified v-AuNWs electrode

v-AuNWs based stretchable electrode was fabricated through a seed-mediated method according to our previously published reports (Zhai et al., 2018, 2020a). In brief, a thin layer of poly(methyl methacrylate) (PMMA) was first spun onto the surface of Si wafer, which was followed by O_2 plasma treatment. Then the PMMA/Si substrate was successively immersed in ethanol solution containing (3-Aminopropyl)triethoxysilane (APTES) and Au nanoparticles solution for an hour each. This step led to a sub-monolayer of Au nanoparticles on the PMMA surface. After rinsing with water and being dried by blowing with N_2, the Au/PMMA/Si was finally immersed in the nanowire growth solution containing ethanol, Au source ($HAuCl_4$), 4-mercaptobenzoic acid (MBA) for 5 min. After drying with N_2, a thin layer of PDMS was subsequently spun onto the surface of v-AuNWs/PMMA/Si substrate followed by annealing in an oven (60°C) overnight. Upon removal of PMMA, free-standing v-AuNWs embedded PDMS sheet was obtained. The standing and vertically aligned structures of AuNWs were evident as confirmed by scanning electron microscopy (SEM)

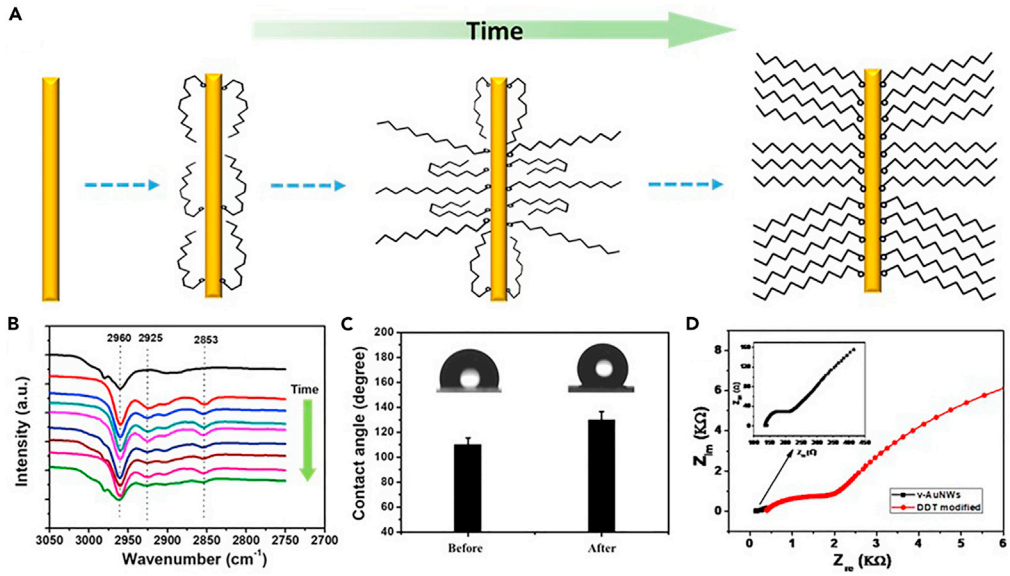

Figure 2. Schematic illustration and characterizations of the self-assembly kinetics of DDT

(A) Schematic illustration of the self-assembly kinetics of DDT on the surface of v-AuNWs with the increasing reaction time.

(B) FTIR spectrum of v-AuNWs stretchable electrodes at different DDT treatment time.

(C and D) Contact angels (C) and EIS (D) characterizations of v-AuNWs stretchable electrode before and after DDT modification.

(Figure S2). In addition, the cross-sectional SEM image shows that v-AuNWs were embedded in PDMS (Figure S3), which agrees well with our previous studies (Gong et al., 2019; Lyu et al., 2019; Zhai et al., 2020b).

The PDMS-embedded v-AuNWs were electrically conductive, mechanically stretchable, and could exhibit durable electrical response under multiple stretching/releasing cycles (Lyu et al., 2019; Zhai et al., 2020b). The v-AuNWs electrodes were further modified with DDT SAMs simply by immersing the v-AuNWs electrode into ethanol solution containing 10 mM DDT. Similar to alkyl thiol SAMs formed on a planar bulk gold surface (Vericat et al., 2010), DDT experienced physisorption, chemisorption, crystalline and ordered domains with a closed-packed configuration with the increasing immersion time (Figure 2A). This was proved by the FTIR studies (Figure 2B). The characteristic peaks at 2925 cm^{-1} and 2853 cm^{-1} were ascribed to the CH_2 asymmetric stretching, demonstrating the presence of DDT molecules on the v-AuNWs electrode (Li et al., 2003). With the increase in the modification time, both the peak intensities enhanced, indicating the increasing amount of DDT molecules immobilized onto v-AuNWs.

The successful DDT modification was also proved by the contact angle measurement. As shown in Figure 2C, the water contact angle of the v-AuNWs electrode increased from 109° to 131° after DDT modification. The increase in hydrophobicity was due to the presence of alkyl chains that passivated v-AuNWs surfaces, consistent with the previous result (Pan et al., 1996).

The dynamic self-assembly process of DDT on the v-AuNWs electrode was also characterized with electrochemical probes by cyclic voltammetry (CV) and electrochemical impedance spectroscopy (EIS). In the absence of DDT modification, one-electron redox reaction of $Fe(CN)_6^{3-/4-}$ on the v-AuNWs electrode exhibited the similar CV profile to that on traditional bulk gold surface (black line in Figure S1). Note that the peak-to-peak separation was about 195 mV, which is much greater than the theoretical value of 59 mV on a planar ideal electrode surface. This may be attributed to two factors: (1) v-AuNWs are discontinuous with lower conductivity than corresponding bulk gold electrodes; (2) MBA ligands bonded to v-AuNWs surfaces. Upon DDT modification, the redox currents reduced significantly accompanied with larger peak-to-peak separation. This was because DDT molecules would replace MBA ligands and passivated gold nanowire surfaces more effectively by blocking the efficient electron transfer between the v-AuNWs and $Fe(CN)_6^{3-/4-}$. This blocking effect increased charge-transfer resistance as shown in the EIS characterization

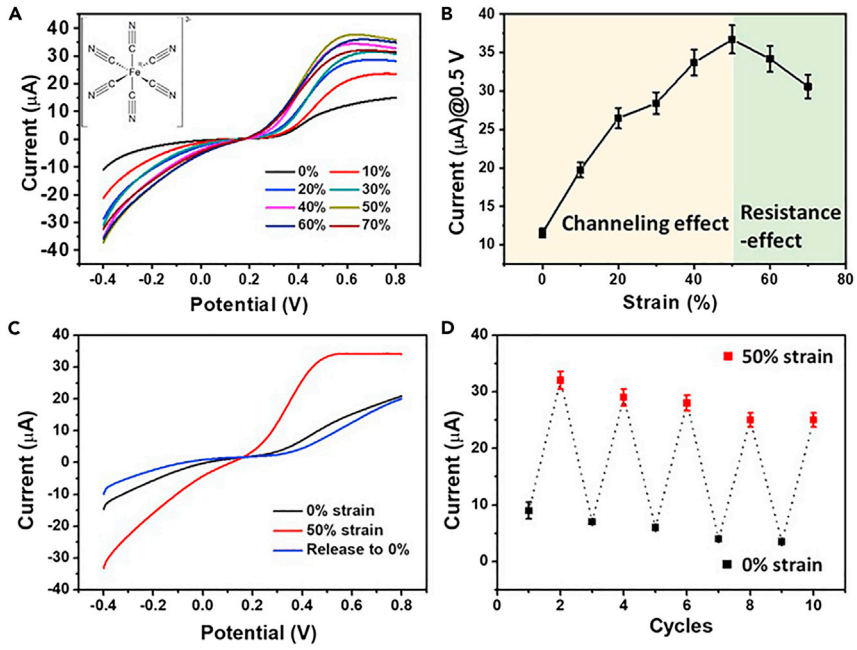

Figure 3. Strain-gated electrochemical ion channel in 5 mM $Fe(CN)_6^{3-/4-}$

(A) LSV curves of the DDT modified v-AuNWs based stretchable electrode under different strains from 0% to 70%.

(B) Plot for strains versus LSV current at 0.5 V *v.s.* Ag/AgCl.

(C) LSV curves of DDT modified v-AuNWs based stretchable electrodes at 0%, 50% and released to 0% stretched states.

(D) The cyclic switching of the current at 0.5 V *v.s.* Ag/AgCl between 0% and 50% strain.

(Figure 2D). The longer the immersion time in DDT solution, the greater level of current reduction was observed until reaching a plateau for a DDT treating time of about 30 min. This is consistent with DDT SAM formation kinetics illustrated in Figure 2A and also in agreement with the FTIR results and the literature (Pan et al., 1996).

Strain-gated redox reactions of $Fe(CN)_6^{3-/4-}$

We further applied mechanical strains to DDT modified v-AuNWs stretchable electrode to investigate how the strain level influenced charge transfers of redox probes ($Fe(CN)_6^{3-/4-}$). As shown in Figure 1B, we expected that the closely-packed v-AuNWs would unzip/crack under mechanical strains, thereby with "opening channels" for charged redox species to penetrate into v-AuNWs matrix. In turn, it would enhance redox current level. This hypothesis was proven in our linear sweep voltammetry (LSV) results presented in Figure 3A. The LSV was used to characterize DDT modified v-AuNWs electrode to "squeeze" strong background capacitance current. Both anodic and cathodic currents increased as the stretch level increased in LSV curves. We further plotted the relationship between the redox current and strains at 0.5 V *v.s.* Ag/AgCl as shown in Figure 3B. It can be clearly seen that the redox current increased with the strain level until a threshold value of about 50% strain. This may be well-interpreted as "ionic channeling effect". Under stains, the closely-packed v-AuNWs would unzip/crack enabling facile penetration of redox ions into v-AuNWs matrix; hence, leading to the increase of Faradaic currents. Nevertheless, it has to be noted that the strain would also cause the decrease of v-AuNW electrode conductivity. Hence, the observed current would be tradeoff between "ionic channeling effect" and "resistance-effect". Between ~50% strain, the former dominated leading to the increase in electrochemical currents; whereas, the later dominated above ~50% strain, resulting in the current decrease.

We characterized morphological structures of v-AuNW electrodes by SEM under different strains from 0% to 70%. As shown in Figure S4, evident cracks were observed on the surface of v-AuNWs electrode as the tensile strains were applied. The sizes of the cracks increased with the strain levels. Nevertheless, the crack-enabled increase in accessible surface area to ionic electrochemical probes couldn't explain the substantial increase in redox currents (at least 3.5 times). Hence, the inter-nanowire spacing likely increased upon

external strains applied, consistent with our early studies (Wang et al., 2018a). On the other hand, the cracks induced by mechanical strain led to a decrease in conductivity of v-AuNWs conductor as a result of reduced wire-to-wire connectivity. Hence, the observed current would be a tradeoff between increased accessibility to redox probes and decreased conductivity of DDT-modified v-AuNWs. The former dominated for the strain level below about 50%, whereas the latter dominated for the larger strain level.

The mechanically gated electrochemical behaviors were reversible. This was demonstrated for the current switching between 0% and 50% strain in the solution of $Fe(CN)_6^{3-/4-}$ as shown in Figure 3C. When the 50% strain was released to 0%, the LSV line shape almost recovered to the one before the stretching applied albeit both anodic and cathodic currents were even smaller. This may be attributed to reduced conductivity upon strain release. Moreover, the current at 0.5 V *v.s.* Ag/AgCl could be switched reversibly between 0% and 50% with multiple cycles (Figure 3D). This electrochemical reversibility is in good agreement with morphological changes as demonstrated by SEM images as shown in Figure S2. At the non-strained "off" state, there were barely any observable cracks on the stretchable electrode. But when 50% strain was applied, large cracks were observed, corresponding to electrochemical "open" state. Upon strain release to 0% strain, all the cracks were also gone recovering the initial morphology, indicating minimal delamination consistent with previous reports (Wang et al., 2018b; Zhai et al., 2020b). In addition, the long-term durability of the fabricated mechanically-gated electrochemical ionic channel was also investigated by recording and comparing the switch behavior before and after repeatedly applying/releasing 50% strain for every 20 cycles. As shown in Figure S5, the fabricated electrochemical ionic channel exhibited good mechanical switching properties even after repeatedly applying/releasing 50% strain for 100 cycles, demonstrating its good long-term durability and stability. The slight drifting of on/off currents might be because of v-AuNWs cracking under repeating strain/release.

Furthermore, a control experiment was firstly performed on v-AuNWs stretchable electrode without DDT modification in 5 mM $Fe(CN)_6^{3-/4-}$. A completely opposite experimental result was obtained in comparison with DDT modified v-AuNWs stretchable electrodes. As seen in Figure S6, the redox peak current decreased along with the applied strains from 0% to 60% together with gradually increasing peak separation, which was attributed to decreased conductivity (Zhai et al., 2018). Moreover, another control experiment was carried out on a DDT modified sputter-coated bulk gold electrode supported on PDMS. The LSV response current profiles under different strains from 0% to 50% were presented in Figure S7. Evidently, the current decreased with the increase in the applied strains. This decrease in current was a result of strain-induced catastrophic cracks in bulk gold film in sharp contrast with v-AuNWs (Figure S8), which were also proven in our previous report (Wang et al., 2018a, 2018b). The aforementioned control experimental results were summarized in Table S1, which demonstrated the significance of both DDT surface modification and the intrinsically stretchable v-AuNWs electrode to achieve strain-gated Faradaic electrochemical ionic channel behaviors.

Strain-gated redox reactions of $Ru(bpy)_3^{2+}$

Apart from the negative charged redox probes, the electrochemical "on-off" behavior of the proposed mechanically-gated electrochemical switch was also demonstrated for the positive charged redox probes($Ru(bpy)_3^{2+}$). As shown in Figure 4A, the LSV profile for the DDT-modified v-AuNWs electrode without the strain applied featured low current response to voltage sweeping, demonstrating the strong DDT blocking effects toward redox reactions of $Ru(bpy)_3^{2+}$. In contrast, upon the tensile strains applied, the redox currents increased significantly with the strain levels from 10% to 70%. Further scrutiny of the response current at 1.0 V *v.s.* Ag/AgCl indicated a peaking value at about 40% strain, followed by slow decrease with the further strain applied (Figure 4B). This phenomenon shared an analogy to that observed for negatively electrochemical probes (Figure 3B), further demonstrating the tradeoff between strain-induced ionic channeling effect and decreased conductivity.

The mechanically-gated electrochemical switching behaviors were also observed for $Ru(bpy)_3^{2+}$, with evident "on-off" behavior presented in Figure 4C. It can be seen that the redox current increased several folds when a 40% strain was applied. The redox current profile almost recovered to that before the stretching when the strain was released. Slightly lower current profile indicated the increase in electrode resistance during the stretch-release cycle. By monitoring the current at 1.0 V *v.s.* Ag/AgCl, we further proved the reversible "ON" and "OFF" switching between 0% and 40% (Figure 4D).

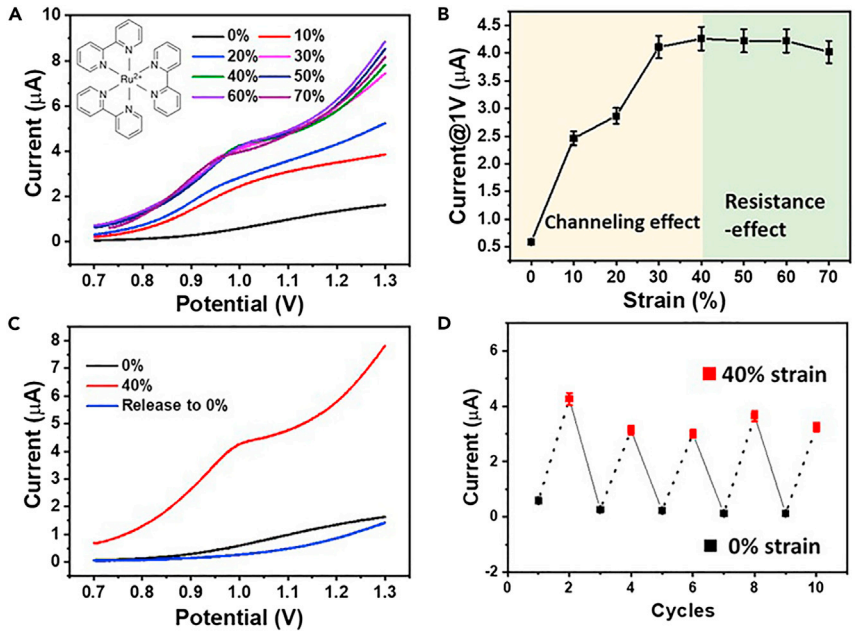

Figure 4. Strain-gated electrochemical ion channel in 2 mM $Ru(bpy)_3^{2+}$

(A) LSV curves of the DDT modified v-AuNWs based stretchable electrode under different strains from 0% to 70%.

(B) Plot for strains versus LSV current at 1.0 V *v.s.* Ag/AgCl.

(C) LSV curves of DDT modified v-AuNWs based stretchable electrodes at 0%, 40% and released to 0% stretched states.

(D)The cyclic switching of the LSV current at 1.0 V *v.s.* Ag/AgCl between 0% and 40% strain.

Conclusions

Unlike bulk electrodes, v-AuNWs are intrinsically stretchable yet electrically conductive. This unique feature, in conjunction with DDT SAMs, allows us to demonstrate a bio-inspired mechanically-gated electrochemical ionic channel. Both the negatively charged redox probe ($Fe(CN)_6^{3-/4-}$) and positively charged redox probe ($Ru(bpy)_3^{2+}$) exhibit an increasing current trend with the increase in strain until reaching a threshold value before the current declining. This is because of the tradeoff between strain-induced "ionic channel opening" and decrease in v-AuNWs conductivity. Furthermore, strain-controlled electrochemical switching is reversible and can be cycled for multiple times. Our findings indicate that the v-AuNWs may serve as a soft bioelectrode for novel applications in real-time monitoring of biological processes such as redox reactions associated with mechanotransduction.

Limitations of the study

The base current on DDT modified v-AuNWs stretchable electrode without the tensile strain applied was still significant. It indicates imperfect DDT blocking charge-transfer reaction. This may be because of the fact that the v-AuNWs surface is rough rendering DDT SAM defective. The use of longer alkyl thiol chains may offer better blocking effects. Further demonstration strain-gated ionic channeling may be directed to smaller redox species and non-charged ones.

STAR★METHODS

Detailed methods are provided in the online version of this paper and include the following:

- KEY RESOURCES TABLE
- RESOURCE AVAILABILITY
  - Lead contact
  - Materials availability
  - Data and code availability
- METHODS DETAILS
  - Fabrication of v-AuNWs based stretchable electrode

- The modification of stretchable electrode
- Fourier transform infrared spectroscopic (FTIR) characterization
- Electrochemical characterization

- QUANTIFICATION AND STATISTICAL ANALYSIS

SUPPLEMENTAL INFORMATION

Supplemental information can be found online at https://doi.org/10.1016/j.isci.2021.103307.

ACKNOWLEDGMENTS

This work is financially supported by ARC discovery projects DP200100624 and DP180101715. This work was performed in part at the Melbourne Center for Nanofabrication (MCN) in the Victorian Node of the Australian National Fabrication Facility (ANFF).

AUTHOR CONTRIBUTIONS

Q.Z. and W.C. conceived and designed the experiments. Q.Z. prepared materials, performed the experiments and wrote the first version of the manuscript. Q.L., R. W., Y. L., S.G. and L. Y participated in characterization, discussion and experimental data analysis. W.C. supervised all the aspects of this work, revised the manuscript and provided financial support. All authors discussed the results and contributed to the paper.

DECLARATION OF INTERESTS

The authors declare no competing interests. Author Wenlong Cheng is a member of the iScience Editorial Board.

Received: June 30, 2021
Revised: September 23, 2021
Accepted: October 15, 2021
Published: November 19, 2021

REFERENCES

Baluška, F., and Mancuso, S. (2009). Plant neurobiology: from sensory biology, via plant communication, to social plant behavior. Cogn. Process. *10*, 3–7.

Courtemanche, M., Ramirez, R.J., and Nattel, S. (1998). Ionic mechanisms underlying human atrial action potential properties: insights from a mathematical model. Am. J. Physiol. Heart Circ. Physiol. *275*, H301–H321.

Delmas, P., and Coste, B. (2013). Mechano-gated ion channels in sensory systems. Cell *155*, 278–284.

Dong, S., and Li, J. (1997). Self-assembled monolayers of thiols on gold electrodes for bioelectrochemistry and biosensors. Bioelectrochem. Bioenerg. *42*, 7–13.

Gong, S., Yap, L.W., Zhu, B., Zhai, Q., Liu, Y., Lyu, Q., Wang, K., Yang, M., Ling, Y., and Lai, D.T. (2019). Local crack-programmed gold nanowire electronic skin tattoos for in-plane multisensor integration. Adv. Mater. *31*, 1903789.

Huang, W., Zhang, Z., Han, X., Tang, J., Wang, J., Dong, S., and Wang, E. (2002). Ion channel behavior of amphotericin B in sterol-free and cholesterol-or ergosterol-containing supported phosphatidylcholine bilayer model membranes investigated by electrochemistry and spectroscopy. Biophys. J. *83*, 3245–3255.

Li, Z., Chang, S.-C., and Williams, R.S. (2003). Self-assembly of alkanethiol molecules onto platinum and platinum oxide surfaces. Langmuir *19*, 6744–6749.

Lyu, Q., Zhai, Q., Dyson, J., Gong, S., Zhao, Y., Ling, Y., Chandrasekaran, R., Dong, D., and Cheng, W. (2019). Real-time and in-situ monitoring of H_2O_2 release from living cells by a stretchable electrochemical biosensor based on vertically aligned gold nanowires. Anal. Chem. *91*, 13521–13527.

Pan, W., Durning, C., and Turro, N. (1996). Kinetics of alkanethiol adsorption on gold. Langmuir *12*, 4469–4473.

Pappa, A.-M., Liu, H.-Y., Traberg-Christensen, W., Thiburce, Q., Savva, A., Pavia, A., Salleo, A., Daniel, S., and Owens, R.M. (2020). Optical and electronic ion channel monitoring from native human membranes. ACS Nano *14*, 12538–12545.

Ranade, S.S., Syeda, R., and Patapoutian, A. (2015). Mechanically activated ion channels. Neuron *87*, 1162–1179.

Reeh, P.W. (1986). Sensory receptors in mammalian skin in an in vitro preparation. Neurosci. Lett. *66*, 141–146.

Vericat, C., Vela, M., Benitez, G., Carro, P., and Salvarezza, R. (2010). Self-assembled monolayers of thiols and dithiols on gold: new challenges for a well-known system. Chem. Soc. Rev. *39*, 1805–1834.

Wang, K., Lin, F., Lai, D.T., Gong, S., Kibret, B., Ali, M.A., Yuce, M.R., and Cheng, W. (2021). Soft gold nanowire sponge antenna for battery-free wireless pressure sensors. Nanoscale *13*, 3957–3966.

Wang, Y., Gong, S., Gomez, D., Ling, Y., Yap, L.W., Simon, G.P., and Cheng, W. (2018a). Unconventional Janus properties of enokitake-like gold nanowire films. ACS Nano *12*, 8717–8722.

Wang, Y., Gong, S., Wang, S.J., Yang, X., Ling, Y., Yap, L.W., Dong, D., Simon, G.P., and Cheng, W. (2018b). Standing enokitake-like nanowire films for highly stretchable elastronics. ACS Nano *12*, 9742–9749.

Wu, Z., Tang, J., Cheng, Z., Yang, X., and Wang, E. (2000). Ion channel behavior of supported bilayer lipid membranes on a glassy carbon electrode. Anal. Chem. *72*, 6030–6033.

Yap, L.W., Shi, Q., Gong, S., Wang, Y., Chen, Y., Zhu, C., Gu, Z., Suzuki, K., Zhu, Y., and Cheng, W. (2019). Bifunctional Fe_3O_4@ AuNWs particle as wearable bending and strain sensor. Inorg. Chem. Commun. *104*, 98–104.

Zhai, Q., and Cheng, W. (2019). Soft and stretchable electrochemical biosensors. Mater. Today Nano *7*, 100041.

Zhai, Q., Gong, S., Wang, Y., Lyu, Q., Liu, Y., Ling, Y., Wang, J., Simon, G.P., and Cheng, W. (2019). Enokitake mushroom-like standing gold nanowires toward wearable noninvasive bimodal glucose and strain sensing. ACS Appl. Mater. Interfaces *11*, 9724–9729.

Zhai, Q., Liu, Y., Wang, R., Wang, Y., Lyu, Q., Gong, S., Wang, J., Simon, G.P., and Cheng, W. (2020a). Intrinsically stretchable fuel cell based on enokitake-like standing gold nanowires. Adv. Energy Mater. *10*, 1903512.

Zhai, Q., Wang, Y., Gong, S., Ling, Y., Yap, L.W., Liu, Y., Wang, J., Simon, G.P., and Cheng, W. (2018). Vertical gold nanowires stretchable electrochemical electrodes. Anal. Chem. *90*, 13498–13505.

Zhai, Q., Yap, L.W., Wang, R., Gong, S., Guo, Z., Liu, Y., Lyu, Q., Wang, J., Simon, G.P., and Cheng, W. (2020b). Vertically aligned gold nanowires as stretchable and wearable epidermal ion-selective electrode for noninvasive multiplexed sweat analysis. Anal. Chem. *92*, 4647–4655.

STAR★METHODS

KEY RESOURCES TABLE

REAGENT or RESOURCE	SOURCE	IDENTIFIER
Chemicals		
(3-Aminopropyl)triethoxysilane (APTES),	Sigma-Aldrich	440140, CAS 919-30-2
Gold(III) chloride trihydrate ($HAuCl_4$)	Sigma-Aldrich	520918, CAS 16961-25-4
Sodium borohydride ($NaBH_4$)	Sigma-Aldrich	452882, CAS 16940-66-2
Sodium citrate	Sigma-Aldrich	S4641, CAS 6132-04-3
L-ascorbic acid	Sigma-Aldrich	255564, CAS 50-81-7
4-Mercaptobenzoic acid (MBA)	Sigma-Aldrich	706329, CAS 1074-36-8
potassium ferricyanide ($K_3[Fe(CN)_6]$)	Sigma-Aldrich	702587, CAS 13746-66-2
potassium ferrocyanide ($K_4[Fe(CN)_6]$)	Sigma-Aldrich	P3289, CAS 14459-95-1
Tris(2,2′-bipyridine)ruthenium(II) chloride hexahydrate ($Ru(bpy)_3Cl_2$)	Sigma-Aldrich	544981, CAS 50525-27-4
1-Dodecanethiol (DDT)	Sigma-Aldrich	471364, CAS 112-55-0
Poly(methyl methacrylate) (PMMA)	MicroChem Corp. (Westborough, USA).	950 A6
PDMS base and curing agent	Dow Corning	Sylgard 184
Software and algorithms		
OriginLab	OriginLab Corporation	https://www.originlab.com/
Image J	Rasband, 1997-2018	https://imagej.nih.gov/ij/

RESOURCE AVAILABILITY

Lead contact

Further information and requests for resources and reagents should be directed to and will be fulfilled by the Lead Contact, Wenlong Cheng (wenlong.cheng@monash.edu).

Materials availability

This study did not generate new unique reagents.

Data and code availability

- All data reported in this paper will be shared by the lead contact upon request.
- This paper does not report original code.
- Any additional information required to reanalyze the data reported in this paper is available from the lead contact upon request.

METHODS DETAILS

Fabrication of v-AuNWs based stretchable electrode

v-AuNWs embedded in PDMS was obtained according to our recently reported seed-mediated method, and the experimental processes were described in detail as following.

(1) Synthesis of Au nanoparticle seeds

Sodium citrate protected Au nanoparticles suspensions were prepared by reducing 0.25 mM $HAuCl_4$ in aqueous solution using $NaBH_4$ (6 mM) in the presence of sodium citrate (0.5 mM).

(2) Surface treatment of Silicon wafer

Firstly, a thin layer of PMMA was spin-coated on the surface of Si wafer at the speed of 3000 rpm for 50s, then transferred to a hotplate that baked at 180°C for 2 minutes. After cooling to room temperature, PMMA/Si wafter was treated by O_2 plasma for 5 min, and then immersed in absolute ethanol solution containing 5 mM APTES for 2 h. Finally, the water was rinsed with ethanol to remove weakly bonded APTES and dried by N_2.

(3) Au nanoparticles attachment

The above APTES modified PMMA/Si wafter was immersed in Au seeds (10 nm) solution for about 2 h. The negative charged Au nanoparticles would be adsorbed on the positive charged APTES modified PMMA/Si wafter surface through electrostatic interaction. Then the substrate was rinsed with water and dried by N_2.

(4) AuNWs growth

Au nanoparticles attached PMMA/Si wafter was immersed in v-AuNWs growth solution containing 12 mM $HAuCl_4$, 1 mM MBA, 30 mM L-AA for 3 min, then rinsed with ethanol and dried by N_2.

(5) Spin-coating PDMS

PDMS with the base and curing agent ratio of 10:1 (w/w) was spin-coated on the surface of PMMA/Si wafter with v-AuNWs at 500 rpm for 30 s. The coated PDMS was cured in an oven overnight at 60°C. Finally, the v-AuNWs based stretchable electrode array was obtained by dissolving the sacrificial layer of PMMA in acetone.

The modification of stretchable electrode

The above obtained stretchable electrode was immersed in 1 mM DDT ethanol solution for different treatment times, and then rinsed with ethanol to remove the excessive DDT, dried by N_2 for characterization.

Fourier transform infrared spectroscopic (FTIR) characterization

FTIR analysis of the unmodified and DDT modified v-AuNWs based stretchable electrode was carried out using a Vertex 80 FTIR spectrometer (Bruker, Germany). The FTIR spectra were recorded over the scanning range of 2750–3050 cm^{-1} at room temperature.

Electrochemical characterization

Cyclic voltammetry (CV) and Linear Sweep Voltammetry (LSV) characterization of v-AuNWs based stretchable electrode (fixed on a homemade stretching device) under different stretched states were performed by an electrochemical workstation (VersaSTAT3, Princeton Applied Research). In 5 mM $Fe(CN)_6^{3-/4-}$ aqueous solution, the scan range was from −0.4 V to 0.8 V with the scan rate of 50 mV/s; In 2 mM $Ru(bpy)_3^{2+}$ aqueous solution, the scan range was from 0.7 V to 1.3 V with the scan rate of 50 mV/s. Electrochemical impedance spectroscopy (EIS) was carried out in 5 mM $Fe(CN)_6^{3-/4-}$ solution containing 0.1 M KCl, and the frequency from 10^5 Hz to 1 Hz.

QUANTIFICATION AND STATISTICAL ANALYSIS

All averaged datasets, are averages of at least 3 times test and are reported as mean ± standard deviation. SEM Statistical analysis was performed through Image J.